Cellular Immunology 346 (2019) 103929

Contents lists available at ScienceDirect

Cellular Immunology

journal homepage: www.elsevier.com/locate/ycimm

Analysis of macrophages and neutrophils infiltrating murine mammary carcinoma sites within hours of tumor delivery

Chenyu Zhang, Matthew Adusei, Alison Baranovic, Matthew DeBenedetto, Amanda Lauricella, Silvia Chilel Martin, Catherine Newsom-Stewart, Jennifer Schwartz, Robert A. Kurt*

Department of Biology, Lafayette College, Easton, PA 18042, USA

ARTICLE INFO

Keywords:
Murine mammary carcinoma
4T1
EMT6
168
Macrophages
Neutrophils

ABSTRACT

Here we used three different murine mammary carcinomas to study the immune environment associated with early tumor sites. While it was not surprising that the early immune response was predominated by macrophages and neutrophils, there were some novel findings at this early stage of disease. For instance, the macrophages and neutrophils expressed a mixed cytokine profile with TNF-α and TGF-β both produced at appreciable levels. Moreover, while the cells retained their phagocytic capacity, production of reactive oxygen species by the macrophages and neutrophils was in decline. Alterations in the metabolic profile of the tumor associated macrophages were also evident with a decrease in the ATP production rate, and a higher dependence on oxidative phosphorylation for ATP production. Collectively, these data indicate a mixed phenotype of tumor-associated macrophages and neutrophils evident within hours of murine mammary carcinoma delivery.

1. Introduction

Myeloid cells are among the first cells to arrive at a tumor site, and the importance of having a thorough understanding of these cells is underscored by clinical data which reveal that tumor associated macrophages and neutrophils correlate with poor prognosis [1–10], and negatively impact efficacy of checkpoint inhibitor therapy in patients with cancer [11–14].

Tumor associated macrophages may fall into two broad categories; M1 are generally considered beneficial in the immune response against cancer and express factors such as iNOS, IL-12, and TNF-α [15], while M2 are generally considered pro-tumorigenic and express factors such as arginase, MMP-9, and TGF-β [15], and investigations are underway to determine how to selectively deplete and/or convert M2 to M1 macrophages [16–19]. The ability to maximize the beneficial aspects of M1 macrophages, and minimize the detrimental aspects of M2 macrophages in a cancer setting could benefit from a greater understanding of how macrophages are polarized. While there is a good understanding of how to polarize these cells *in vitro* [20], exactly when, and how M2 macrophages arise in murine cancer models or patients with cancer has yet to be well-defined. While studies have reported that factors such as oncostatin M and mTOR signaling, as well as hypoxia, contribute to M2 polarization [21,22], the impact of the microenvironment on metabolism and effector function is another active area of investigation [23–25]. However, there remains a paucity of information about macrophages that arrive at early tumor sites, which is unfortunate because the earlier one intervenes, the more likely it is that polarization or the pro-tumor phenotype can be prevented or reversed. As a case in point, Kim et al. [26] showed that myeloid derived suppressor cells can recover their antigen presenting cell activity if treated with retinoic acid early, but they could not be rescued at later stages of disease progression.

Some investigations also support the contention that tumor associated neutrophils should be categorized into two types, where N1 are considered beneficial in the immune response against cancer since they are cytotoxic and express factors such as iNOS, IL-12 and TNF-α, while N2 are considered pro-tumorigenic and contribute to angiogenesis, invasion, and immune suppression by expressing factors such as arginase, CCL2, CCL5, and IL-10 [27]. Similar to macrophages, the neutrophil response may depend upon tumor type and stage of disease progression. For example, in the RIP-TAG model depleting neutrophils resulted in slower tumor growth, likely a consequence of depleting a major source of MMP-9 thus preventing the angiogenic switch [28].

Although tumor associated macrophages and neutrophils can contribute to cancer progression, most of what we know about their role in cancer comes from analysis of these cells isolated from advanced tumors, or the periphery of humans or mice at advanced stages of disease. These studies have largely led to a model in which tumor progression

* Corresponding author.
E-mail address: kurtr@lafayette.edu (R.A. Kurt).

https://doi.org/10.1016/j.cellimm.2019.103929
Received 31 May 2019; Accepted 2 June 2019
Available online 04 June 2019

over time creates an environment that leads to the generation of pro-tumor macrophages and neutrophils which then further potentiates tumor progression. However, alterations in myeloid cells are underway at early stages of tumor growth, before a tumor is even palpable, indicating a need for more information about phenotype and function of macrophages and neutrophils at early tumor sites. Remarkably, analysis at an early time point is practical, to some extent, in patients. For example, ductal carcinoma *in situ* (DCIS) has been used to investigate characteristics of the site that correlate with disease progression [29–31], and McKee et al. [32] reported almost 20 years ago that the presence of macrophages were among the characteristics for high grade DCIS. More recently, Degnim et al. [33] found macrophages were among the most common infiltrating white blood cells in many DCIS specimens, and Campbell et al. [34] reported CD8+ T cells and macrophages were associated with risk of recurrence. While studies further characterizing macrophages at sites of DCIS are ongoing, Hung et al. [35] found M1 and M2 macrophages in the circulation of patients with DCIS supporting the contention that these cells are present at early stages of disease. Yet, unfortunately, we still do not have a clear understanding of what the macrophages are doing at this early stage of disease.

Although it is hard to capture and characterize macrophages from early tumor sites, several animal studies support the contention that pro-tumor macrophages are present at early tumor sites. For instance, Riabov et al. [36] used matrigel to capture macrophages 7 days after tumor delivery and found a mixture of M1 and M2 phenotypes. And, Carron et al. [37] used a p53-/-mammary carcinoma model and reported an increase in pro- and anti-tumor macrophages before the tumor was even palpable. Notably, the authors also reported that macrophages present at this early stage of disease contributed to tumor progression [37]. What is more, a pro-tumor phenotype at these early time points cannot be explained by a hypoxic environmental (the tumors are not yet 2–3 mm^3) or chronic inflammation; factors often attributed with the generation of macrophages with a pro-tumor phenotype. These data underscore the need to gain a stronger foundational understanding of myeloid cells that arrive early at tumor sites.

In this study we used a gelfoam model [38–40] to capture macrophages and neutrophils from early tumor sites (24–72 h post injection) to gain information about their phenotype, function, and metabolism. Our data indicate that distinct innate immune profiles to different murine mammary carcinomas are evident within hours of tumor delivery, and that the macrophages and neutrophils display a mixed phenotype that incorporates both pro- and anti-tumor characteristics at early tumor sites regardless of the aggressiveness or immunogenicity of the tumor.

2. Material and methods

2.1. Cells and mice

4T1, EMT6, and 168 murine mammary carcinomas were maintained in complete RPMI (cRPMI) (RPMI 1640, Lonza, Walkersville, MD) supplemented with 10% heat-inactivated fetal bovine serum (Lonza), glutamine (2 mM, Lonza), penicillin (100 U/mL, Lonza), streptomycin (100 μg/mL, Lonza), nonessential amino acids (Sigma, St. Lois, MO), 2-mercaptoethanol (5×10^{-5} M, Sigma), and sodium pyruvate (1 mM, Lonza). Balb/c mice were bred on site and were housed in a thoren caging system (Thoren Caging Systems Inc., Hazelton, PA). Food and water were provided *ad libitum*. All mice were used in accordance with an Institutional Animal Care and Use Committee approved protocol that followed the guidelines for ethical conduct in care and use of animals.

2.2. Gelfoam implantation, injections, and recovery

Mice were anesthetized in a chamber with 2–3% isoflurane for 5 min and then maintained on isoflurane throughout the surgery via nosecone delivery. Once anesthetized the mice were shaved, wiped with alcohol and iodine pads, and a small incision was made in the back of the animals. Gelfoam (~10 mm × 10 mm, Pfizer, New York, NY) was inserted under the skin, wounds clips were used to seal the wound, and all mice were monitored for full recovery. Two days later the mice were anesthetized once again and HBSS (Lonza) or the tumor cells ($5x10^4$ 4T1, 1×10^5 EMT6, or 2×10^5 168) were delivered into the gelfoam implant. Twenty four to 72 h later the gelfoam implants were removed and digested in a collagenase cocktail (1 mg/ml collagenase type IV, 10 U/ml hyaluronidase, 20 mg/L DNase, Worthington Biochemical Corp, Lakewood, NJ) for 2 h at room temperature while rocking. The cells were filtered through 50 μM nytex and following red blood cell lysis, the cells were counted.

2.3. Cell staining and flow cytometry

Following isolation from the early tumor sites cells were labeled with antibodies for macrophages (F4/80 (PE)), neutrophils (Ly6G (FITC), natural killer cells (CD49b (PE)), helper T cells (CD3 (FITC)/CD4 (PE)), and cytotoxic T cells (CD3 (FITC)/CD8 (PE)). Separate samples were treated with the appropriate isotype controls. All antibodies were purchased from BD Biosciences (San Diego, CA). For labeling, cells were resuspended in staining buffer (1× phosphate buffered saline, 2% fetal bovine serum, 0.09% sodium azide) and 1×10^6 cells/tube were incubated with Fc block (anti-CD16/CD32, BD Biosciences) for 15 min on ice. Next, 1 μg of the specific antibodies were added and the cells were incubated for 30 min on ice. Following a wash with staining buffer the cells were resuspended in 0.5 ml HBSS and analyzed on a BD FACS Melody flow cytometer.

2.4. Intracellular cytokine analysis

For intracellular cytokine analysis cells were treated with GolgiPlug (BD Biosciences) for 6 h at 37 °C, washed with staining buffer, and then resuspended in 1 ml staining buffer and treated with Fc block for 15 min on ice. After surface staining with antibodies for Ly6G (BV711, BD Biosciences) and F480 (APC, BioLegend, San Diego, CA) for 30 min on ice, the cells were washed two times, resuspended in 250 μl fixation/permeabilization buffer (BD Biosciences) and incubated for 20 min on ice. Following two washes with perm/wash buffer (BD Biosciences) cells were labeled with antibodies for TNF-α (APC-Cy7, BD Biosciences), TGF-β (BV421, BD Biosciences), iNOS (Alexa-488, ThermoFisher, Waltham, MA), Arginase (PE, R&D Systems, Minneapolis, MN) or the appropriate isotype controls for 30 min on ice. Following one wash with perm/wash buffer the cells were incubated with 3.7% paraformaldehyde (Sigma) for 10 min on ice, washed again, and then resuspended in 0.5 ml HBSS. The samples were sent for analysis to the Cell Science Core Facility at Penn State College of Medicine, Hershey Medical Center.

2.5. ROS assay

For analysis of reactive oxygen species 1×10^6 cells were resuspended in 1 ml of staining buffer, 10 μl of 2′,7′-Dichlorodihydrofluorescein diacetate (DCFDA, 2 μM final concentration, VWR) was added, and the cells were incubated for 30 min at 37 °C. Following two washes with staining buffer the cells were incubated with Fc block for 5 min on ice and then anti-Ly6G (PE) or anti-F4/80 (PE) antibodies for 20 min on ice. Next, the cells were washed one time with staining buffer, resuspended in 0.5 ml staining buffer, and then analyzed on a BD FACS Melody flow cytometer.

2.6. Phagocytosis assay

For analysis of phagocytosis 1×10^6 cells were resuspend in 1 ml of staining buffer, 10 μl *E. coli* bioparticles (Alexa-488 conjugated, ThermoFisher) were added, and the cells were incubated for 30 min at 37 °C. Following two washes with staining buffer the cells were

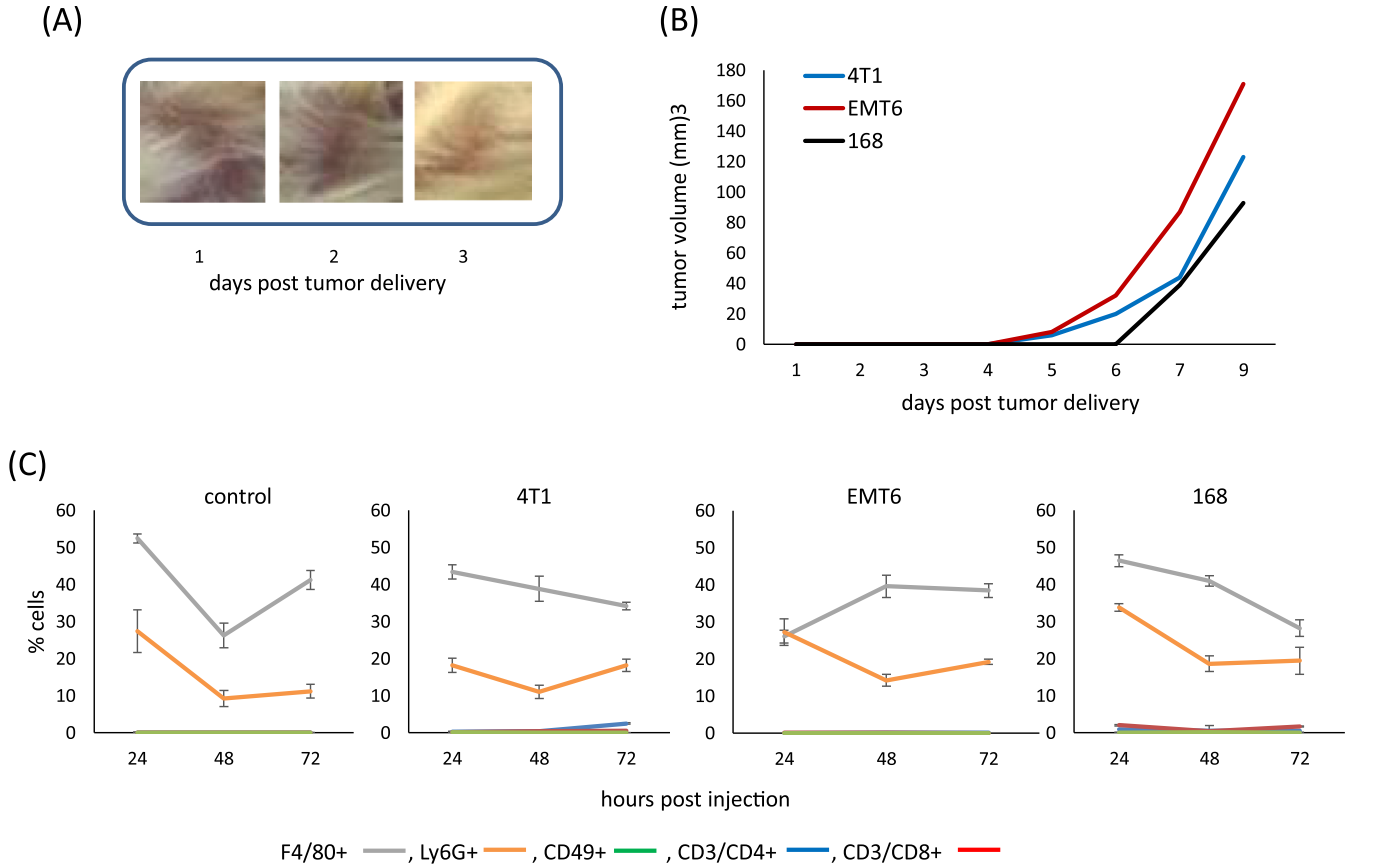

Fig. 1. Capturing cells from early tumor sites. (A, B) 4T1, EMT6 and 168 murine mammary carcinomas are not palpable within the first few days after tumor delivery. (C) A gelfoam model was used to capture and analyze white blood cells infiltrating control (saline) and early tumor sites 24 to 72 h after delivery. The majority of cells were F4/80$^+$ and Ly6G$^+$ with little to no NK (CD49$^+$) cells or T cells. Five mice were used for each group for each experiment at each time point, and all data represent the average and standard error of at least three separate experiments.

incubated with Fc block for 5 min on ice, and then anti-Ly6G (PE) or anti-F4/80 (PE) antibodies for 20 min on ice. Next, the cells were washed one time with staining buffer, resuspended in 0.5 ml staining buffer, and then analyzed on a BD FACS Melody flow cytometer.

2.7. Seahorse assays

To hydrate the XFp sensor cartridge (Agilent Technologies, Cedar Creek, TX), each well of the plate and the surrounding moats were filled with 200 µL and 400 µL of sterile distilled water respectively. The cartridge/utility plate assembly was incubated in a humidified non-CO_2 37 °C incubator overnight. On the day of assay, 45 min prior to loading drug ports, the water in the wells and moats was replaced with the XF Calibrant (Agilent Technologies) of the same volume and allowed to equilibrate in a non-CO_2 37 °C incubator. The assay media was prepared a day prior to the assay by adding 1 mM sodium pyruvate (Lonza), 2 mM L-glutamine (Lonza), and 10 mM glucose (Sigma Aldrich, St. Louis, MO) to pre-warmed XF DMEM pH 7.4 media (Agilent Technologies). The Seahorse Glycolytic Rate Assay (Agilent Technologies) was combined with an additional injection of oligomycin A (Abcam, Cambridge, MA) in order to enable calculation of glycolytic rates and ATP production rates from the OXPHOS and glycolysis pathways. The oligomycin A stock was prepared by resuspending in ethanol to 100 µM and subsequently diluting in Seahorse assay media to a final concentration of 1.5 µM per well. The rotenone plus antimycin A (Rot/AA) stock of 25 µM was diluted in Seahorse assay media to a final concentration of 0.5 µM per well, and the 2-deoxy-D-glucose (2-DG) stock of 500 mM was diluted in Seahorse assay media to a final concentration of 50 mM per well. The drugs were loaded into the drug ports on the Seahorse cartridge, with oligomycin going into port A (20 µL), Rot/AA into port B (22 µL), and 2-DG into port C (25 µL). On the day of the assay, cells were resuspended at 2×10^5 cells/well in Seahorse assay media in a total volume of 180 µL and seeded onto the Seahorse XFp cell culture miniplates. The plates were then centrifuged at 335 × *g* for 2 min and checked for confluency. Next, the cell culture plates were incubated in a humidified non-CO_2 37 °C incubator 45 min to remove residual acid traces from external sources of CO_2. The samples were run using the Seahorse XFp Analyzer (Agilent Technologies) with a modification to the ATP production rate assay protocol. After the initial calibration, three measurement cycles were performed to determine basal rates of glycolysis and OXPHOS. The first injection was oligomycin, followed by an injection of Rot/AA, and then a final injection of 2-DG. Three measurement cycles were conducted after each set of injections, and measurements lasted 18 min, for a total assay run time of 1 h 24 min. Data from the XFp Analyzer were exported as Wave software files as well as EXCEL files. Data analyses were performed on Wave Version 2.6.0.31 to extract information on the rates of Extracellular Acidification Rate (ECAR) (mpH/min) and Oxygen Consumption Rate (OCR) (pmol O_2/min). In the Seahorse ATP production rate report generator, further calculations were performed to determine the glycolytic proton efflux rates (glycoPER) and relative rates of ATP production from the glycolysis and OXPHOS pathways.

3. Results

3.1. The gelfoam system can be used to capture cells associated with early tumor sites

Analysis of the immune response to cancer is often accomplished by capturing white blood cells that infiltrate solid tumors, or isolating cells

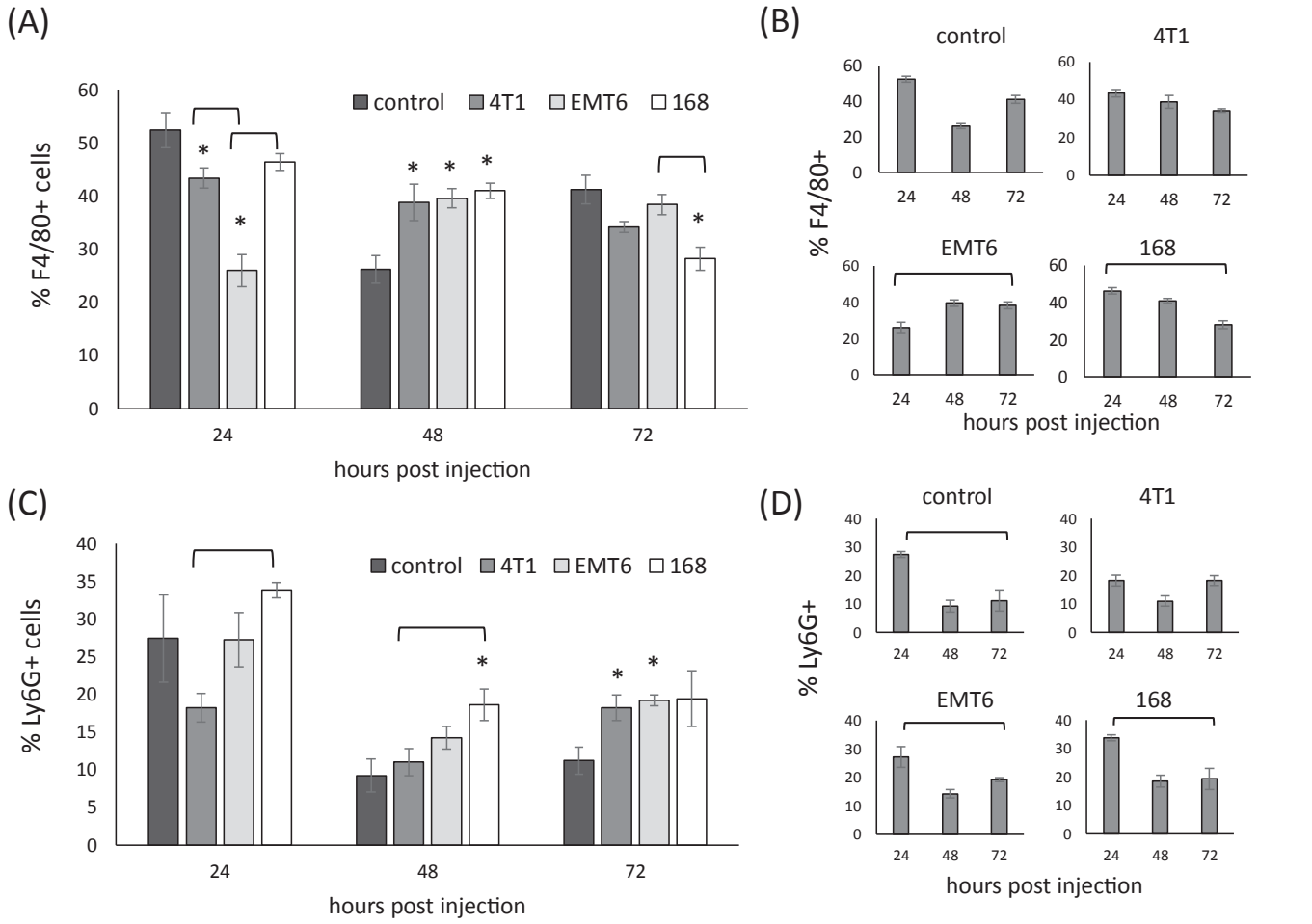

Fig. 2. Significant differences in cell numbers are evident at early tumor sites. Flow cytometric analysis was used to determine the percent of F4/80$^+$ (A, B) and Ly6G$^+$ (C, D) cells present at the tumor sites 24 to 72 h after delivery. Five mice were used for each group for each experiment at each time point, and all data represent the average and standard error of at least three separate experiments. (A, C) Where indicated significant differences were found between control and tumor sites (*), and between different tumor sites (⌐¬) $p < 0.05$ using a *Student's t-Test.* (B, D) Where indicated (⌐¬) there were significant changes in cell number over time $p < 0.05$ using ANOVA.

Table 1
Cytokine expression by F4/80$^+$ cells.

		control Mϕ	4T1 Mϕ	EMT6 Mϕ	168 Mϕ
iNOS	24 h	2.6 ± 0.4	2.4 ± 0.5	1.1 ± 0.7	0.6 ± 0.1*
	72 h	1.4 ± 1.1	2.0 ± 1.0	3.3 ± 1.9	0.8 ± 0.2
arginase	24 h	4.7 ± 1.1	4.3 ± 0.2	2.0 ± 0.4‡	3.0 ± 0.9
	72 h	3.0 ± 0.3	5.3 ± 1.7	4.4 ± 0.5	3.3 ± 0.6
TGF-β	24 h	22.8 ± 0.8	24.5 ± 3.7	9.3 ± 2.8*	13.6 ± 3.7
	72 h	17.2 ± 3.0	18.7 ± 6.5	26.9 ± 1.2	15.3 ± 3.4†
TNF-α	24 h	24.1 ± 3.7	25.6 ± 5.4	12.4 ± 3.7	17.8 ± 3.0
	72 h	27.5 ± 1.0	22.7 ± 2.9	41.7 ± 2.7* ‡	31.1 ± 6.2

Red font indicates statistically significant difference ($P < 0.05$) between 24 to 72 h.
*Statistically significant difference ($P < 0.05$) relative to control.
‡Statistically significant difference ($P < 0.05$) relative to 4T1 Mϕ.
†Statistically significant difference ($P < 0.05$) relative to EMT6 Mϕ.

Table 2
Cytokine expression by Ly6G$^+$ cells.

		control PMN	4T1 PMN	EMT6 PMN	168 PMN
iNOS	24 h	1.0 ± 0.3	0.9 ± 0.0	0.3 ± 0.1‡	0.3 ± 0.1‡
	72 h	0.5 ± 0.3	0.8 ± 0.3	0.1 ± 0.1	0.3 ± 0.0
arginase	24 h	1.4 ± 0.4	1.8 ± 0.2	0.9 ± 0.2	0.6 ± 0.1‡
	72 h	0.9 ± 0.1	1.6 ± 0.3	3.3 ± 1.1	0.4 ± 0.2†
TGF-β	24 h	8.4 ± 1.1	7.2 ± 1.1	2.8 ± 0.4*,‡	4.7 ± 0.6
	72 h	5.4 ± 1.1	5.0 ± 1.8	8.1 ± 2.7	3.5 ± 0.9
TNF-α	24 h	6.9 ± 0.5	8.5 ± 2.0	7.3 ± 0.8	6.2 ± 0.1
	72 h	7.9 ± 1.2	8.2 ± 1.2	10.1 ± 1.8	5.0 ± 1.9

* Statistically significant difference ($P < 0.05$) relative to control.
‡ Statistically significant difference ($P < 0.05$) relative to 4T1 PMN.
† Statistically significant difference ($P < 0.05$) relative to EMT6 PMN.

in the periphery of tumor-bearing humans or mice. One difficulty with studying the early immune response to cancer is obtaining enough white blood cells for analysis. As a result there is a paucity of information about the very immune response to cancer; before a tumor is palpable. As a case in point three commonly used murine mammary carcinoma models (4T1, EMT6, 168) are not palpable within the first few days after tumor delivery (Fig. 1A), and it is generally around day 7 before the tumors can be reliably measured (Fig. 1B). In order to study the early immune response to these tumors we employed a gelfoam model [38–40]. In short, mice received a gelfoam implant and two days later saline as a control or tumor cells were injected into the implants. The gelfoam was then removed to capture and analyze the infiltrating white blood cells. For this study we focused on the immune response

evident within the first 72 h following tumor delivery. Antibody labeling revealed that the majority of white blood cells infiltrating early tumor sites, as well as control sites consisted of F4/80$^+$ and Ly6G$^+$ cells (Fig. 1C). Natural killer cells, CD4$^+$, and CD8$^+$ T cells were not detected at appreciable levels. These data show that the early tumor immune environment was predominated by macrophages and neutrophils, and that the gelfoam system can be used to capture cells from early tumor sites for further analysis.

3.2. The number of macrophages and neutrophils at early tumor sites

Analysis of the number of cells infiltrating early tumor sites revealed several significant differences. With respect to macrophages (F4/80$^+$ cells), several of the tumor sites showed fewer macrophages than the control site. For instance, at the 24 h time point there were significantly fewer macrophages at the 4T1 and EMT6 tumor sites compared to the control site, although the trend was reversed at the 48 h time point (Fig. 2A). Significant differences between the tumor sites were also evident. For instance, at the 24 h time point both the 4T1 and 168 tumor sites had significantly more macrophages than the EMT6 tumor site (Fig. 2A). In looking at changes over time there was a significant increase in the number of macrophages at the EMT6 tumor site, and a significant decrease in number of macrophages at the 168 tumor site from 24 to 72 h (Fig. 2B). With respect to neutrophils (Ly6G$^+$ cells), by 72 h all of the tumor sites had more neutrophils than the control site, with significant differences at the 4T1 and EMT6 tumor sites (Fig. 2C). Significant differences across the tumor sites were also evident. For instance, at the 24 and 48 h time points the number of neutrophils at the 168 tumor site was greater than the number of neutrophils at the 4T1 tumor site (Fig. 2C). In looking at changes over time there was a significant decrease in the number of neutrophils at the control, EMT6, and 168 tumor sites (Fig. 2D). Although there were no major trends evident at all three murine mammary carcinoma sites, these data show that within hours of tumor delivery there were several significant differences in the number of macrophages and neutrophils present between the control and tumor sites, and also between the different tumor sites.

3.3. Macrophages and neutrophils at early tumor sites display alterations in effector function

Although there were some significant differences in the number of macrophages and neutrophils present at the early tumor sites, of more significant interest was whether these cells displayed differences in pro- or anti-tumor phenotypes. In order to address this we assessed cytokine production, phagocytic activity, and production of reactive oxygen species (ROS). With the exception of neutrophils from the control site at 24 h, TNF-α was the most predominant cytokine expressed by macrophages and neutrophils at all sites at 24 and 72 h (Tables 1 and 2). For example, 12–25% of macrophages from the 24 h tumor sites were making TNF-α, and the numbers were mostly elevated at the 72 h time point with 22–41% of macrophages making TNF-α (Table 1). Although the cell numbers were lower, a similar pattern was evident for neutrophils. Somewhat surprisingly, a large number of cells also produced TGF-β, and a significant number of macrophages produced both TNF-α and TGF-β, a pattern that may signify undifferentiated cells (Tables 1 and 2, Fig. 3). The number of cells producing iNOS and arginase was quite low at the early tumor sites (Tables 1 and 2). While there were some statistically significant differences in cytokine production between control and tumor sites, and between the different tumor sites, the most notable change in cytokine expression was evident in macrophages at the EMT6 tumor site. At the EMT6 tumor site there was a significant increase in the number of macrophages making arginase, TGF-β and TNF-α between 24 and 72 h (Table 1). At the 24 h EMT6

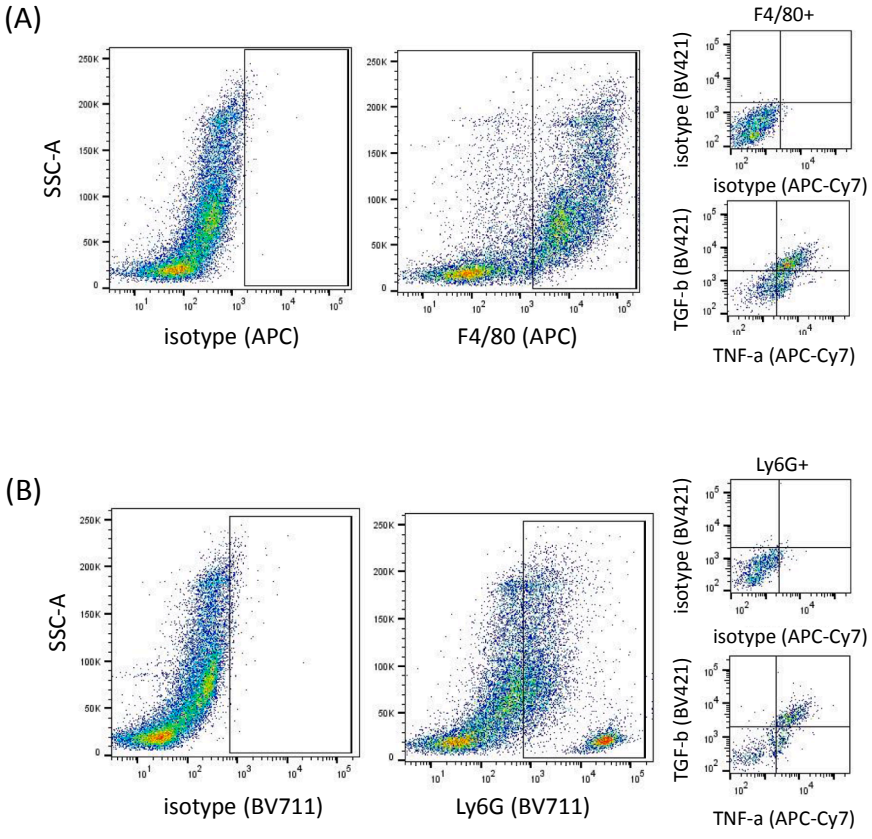

Fig. 3. Intracellular cytokine analysis of macrophages and neutrophils at early tumor sites. Cells were collected from early tumor sites and stained with antibodies specific for F4/80, Ly6G, TNF-α, and TGF-β. The cells were gated on F4/80$^+$ cells (A) and then assessed for TNF-α and TGF-β staining, or gated on Ly6G$^+$ cells (B) and then assessed for TNF-α and TGF-β staining. The data shown are from the 24 h 4T1 tumor site with cells pulled together from five mice, and the data represent one of three separate experiments. Similar staining was evident at the 72 h time point and at the other tumor sites.

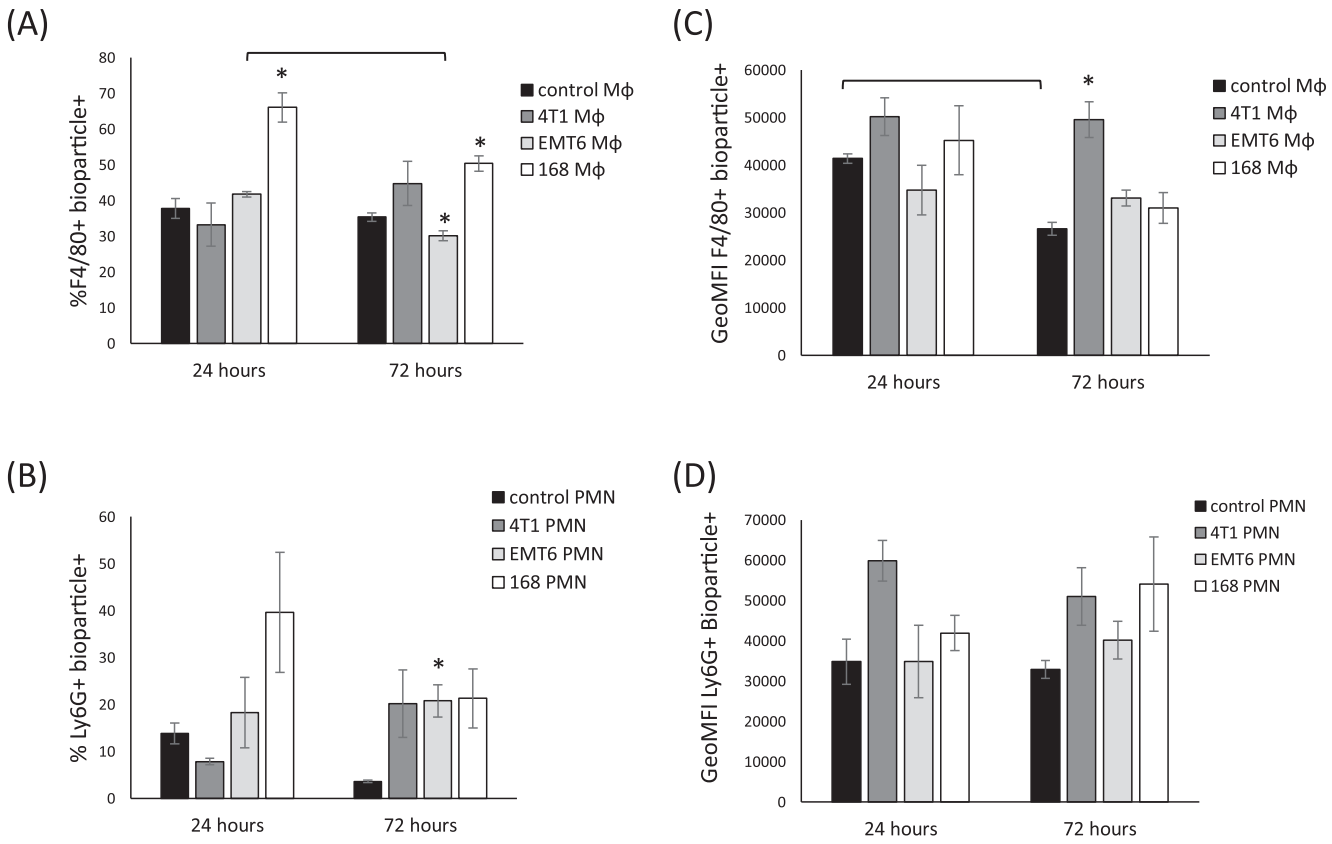

Fig. 4. Phagocytic activity at early tumor sites. Cells were collected from early tumor sites, incubated with fluorescently tagged bioparticles, and then stained with antibodies specific for F4/80 or Ly6G. F4/80$^+$bioparticle$^+$ cells (A) were gated on to assess how many macrophages phagocytosed the bioparticles, and Ly6G$^+$bioparticle$^+$ cells (B) were gated on to assess how many neutrophils phagocytosed the bioparticles. To assess total phagocytic activity we used the GeoMFI of F4/80$^+$bioparticle$^+$ (C), and Ly6G$^+$bioparticle$^+$ (D) cells. Each experiment was conducted with five mice/set at each time point. All data are the average and standard error of at least three separate experiments. Where indicated (*) significant differences were found between control and tumor sites $p < 0.05$ using a *Student's t-Test*. Where indicated (⌐¬) there were significant changes in cell number over time $p < 0.05$ using ANOVA.

tumor site 2% of macrophages were producing arginase, 9% were producing TGF-β, and 12% were producing TNF-α, and these numbers increased to 4%, 26%, and 41% respectively at the 72 h time point.

In order to assess macrophage and neutrophil phagocytic activity we used fluorescently labeled bioparticles. While there were a couple significant differences in the number of phagocytic cells at the tumor sites relative to the control site, the only significant change over time was seen in the number of phagocytic macrophages at the EMT6 tumor site which showed a decrease between 24 and 72 h (Fig. 4A). This was interesting since the number of macrophages at the EMT6 tumor site increased over time (Fig. 2B). To assess phagocytic capacity we analyzed the geometric mean fluorescence intensity (GeoMFI) of the macrophages and neutrophils that had phagocytosed the bioparticles. Here we found that while macrophages at the control site exhibited a significant decrease in phagocytic capacity over time (Fig. 4C), there were no significant changes in the phagocytic capacity of the macrophages or neutrophils at any of the tumor sites over time (Fig. 4C, D). Collectively, these data indicate that myeloid cells at the early tumor sites were capable of phagocytosis, and retained this phagocytic capacity over time while macrophages at the control site exhibited a decrease in their phagocytic capacity.

Next, we looked at ROS production. In general at 72 h there were fewer ROS$^+$ macrophages and neutrophils than there were at 24 h (Fig. 5A, B). However, the results were only significant for macrophages at 168 tumor site, and neutrophils at the control and 168 tumor sites (Fig. 5A, B). On the contrary, there was a significant increase in the number of ROS$^+$ macrophages at the EMT6 tumor site (Fig. 5A). The most striking finding with respect to ROS production came from analyzing how much ROS the cells were producing which was determined using GeoMFI of the ROS$^+$ macrophages and neutrophils. While at 24 h the amount of ROS the macrophages and neutrophils from the tumor sites were making was comparable to the amount of ROS made by macrophages and neutrophils at the control site, by 72 h ROS production was significantly lower at most of the tumor sites compared to the control sites (Fig. 5C, D). Moreover, most of the macrophages and neutrophils at the tumor sites exhibited a significant decrease in ROS production over time (Fig. 5C, D).

3.4. Macrophages at early tumor sites display alterations in metabolism

Finally, because alterations in metabolism of tumor associated macrophages has been reported [6–8,41,42], and because alterations in metabolism are expected to precede alterations in effector function [43], we assessed the metabolic profile of macrophages from the early tumor sites. Assessment of the glycolytic proton efflux rate (GlycoPER) and oxygen consumption rate (OCR) revealed metabolic differences between macrophages at the control and tumor sites. While macrophages at the control site showed increases in the GlycoPER and OCR between 24 and 72 h (Fig. 6A, B), the GlycoPER from macrophages at the tumor sites remained relatively stable over time (Fig. 6A), while the OCR increased in macrophages at the tumor sites (Fig. 6B). Using these data we calculated the ATP production rate and percentage of cells using oxidative phosphorylation (OXPHOS) for their ATP production. There was a significant increase in ATP production from macrophages at the control and 168 tumor sites, but ATP production by macrophages at the 4T1 and EMT6 tumor sites remained unchanged (Fig. 6C). By 72 h ATP production by macrophages at each of the tumor sites was significantly lower than ATP production by macrophages at the control

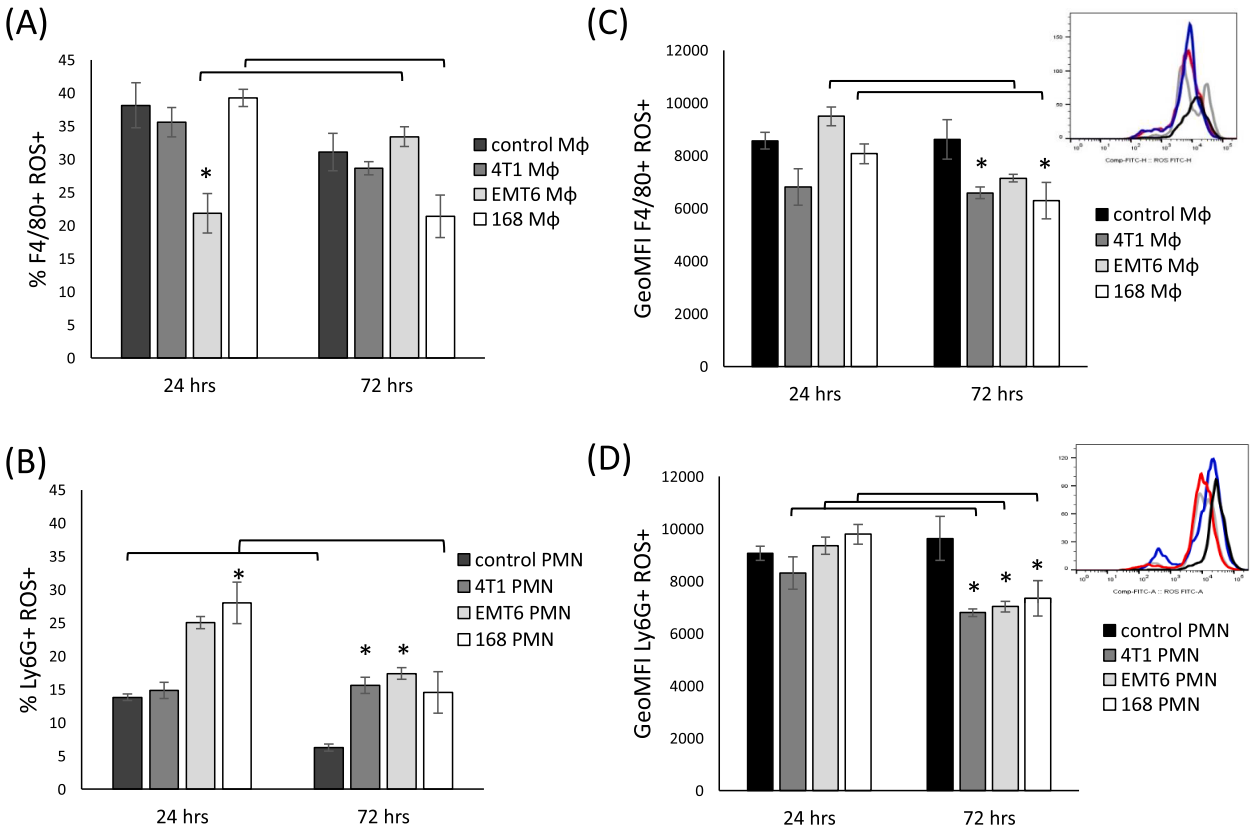

Fig. 5. Production of reactive oxygen species at early tumor sites. Cells were collected from early tumor sites and stained with DCFDA to analyze reactive oxygen species as well as antibodies specific for F4/80 or Ly6G. (A) F4/80$^+$DCFDA$^+$ cells were gated on to assess how many macrophages were producing ROS, and (B) Ly6G$^+$DCFDA$^+$ cells were gated on to assess how many neutrophils were producing ROS. To assess the extent of ROS production we used the GeoMFI of F4/80$^+$DCFDA$^+$ (C), and Ly6G$^+$DCFDA$^+$ (D) cells. Representative histograms from **control**, **4T1**, **EMT6** and **168** sites are shown. All data represent the average and standard deviation of five separate mice from each group at each time point. Where indicated (*) significant differences were found between control and tumor sites $p < 0.05$ using a *Student's t-Test*. Where indicated (⌐¬) there were significant changes in cell number over time $p < 0.05$ using ANOVA.

site (Fig. 6C). With respect to how much OXPHOS was used for ATP production, macrophages at the EMT6 tumor site had the highest level of OXPHOS at the 24 h time point, but only showed a modest increase over time (Fig. 6D). At the 24 h time point OXPHOS in macrophages at two of the tumor sites was significantly higher than OXPHOS in macrophages at the control site, and by 72 h OXPHOS by macrophages at all three of the tumor sites was significantly higher than OXPHOS in macrophages at the control site (Fig. 6D). Due to a lack of sufficient cell recovery a similar analysis of neutrophils was not conducted.

3.5. Assessment of alterations in the context of tumor immunogenicity and aggressiveness

Altogether we found evidence supporting the contention that myeloid cells at sites of early murine mammary carcinomas could not be clearly classified as pro- or anti-tumor. To determine whether changes correlated with tumor aggressiveness or immunogenicity we compiled the most significant findings at the early tumor sites (Fig. 7). Given the 4T1 tumor is considered poorly immunogenic, yet highly metastatic, and the EMT6 tumor is non metastatic but more immunogenic [44,45] one may expect to see myeloid cells with the most pro-tumor phenotype at the 4T1 tumor site, and myeloid cells with the most anti-tumor phenotype at the EMT6 tumor site. Yet, this did not turn out to be the case.

Although the phagocytic capacity of macrophages at the control site significantly decreased over time, the phagocytic capacity of macrophages and neutrophils at the early tumor sites showed no significant changes over time (Fig. 7A). Thus, phagocytic capacity of the tumor associated macrophages and neutrophils was retained at each of the early tumor sites regardless of tumor aggressiveness or immunogenicity. Cytokine expression was only increased at the EMT6 tumor site (Fig. 7B) suggesting that cytokine expression may be correlated with immunogenicity of the tumor, although this conclusion was complicated by the fact that there was an increase in both pro- (TGF-β) and anti-tumor (TNF-α) cytokines. While control cells showed a slight increase in ROS production, there was a significant decrease over time in ROS production by neutrophils at all three tumor sites and macrophage at two of the tumor sites (Fig. 7C) suggesting that these changes were unrelated to aggressiveness and immunogenicity of the tumors. Similarly, there was a significant increase in OXPHOS by 72 h post tumor delivery, at all three tumor sites relative to the control site (Fig. 7D), once again suggesting that these changes were unrelated to aggressiveness or immunogenicity of the tumors. The compiled data also supports the contention that metabolic alterations preceded changes in effector functions in these murine mammary carcinoma models.

4. Discussion

Our initial hypothesis was that macrophages and neutrophils associated with early tumor sites would display an anti-tumor phenotype. Indeed, it has been proposed that anti-tumor macrophages predominate at early stages of cancer and pro-tumor macrophages at later stages [46], and that neutrophils switch from an anti- to a pro-tumor phenotype during cancer progression [47]. The classification of macrophages and neutrophils as pro- or anti-tumor is often based upon several

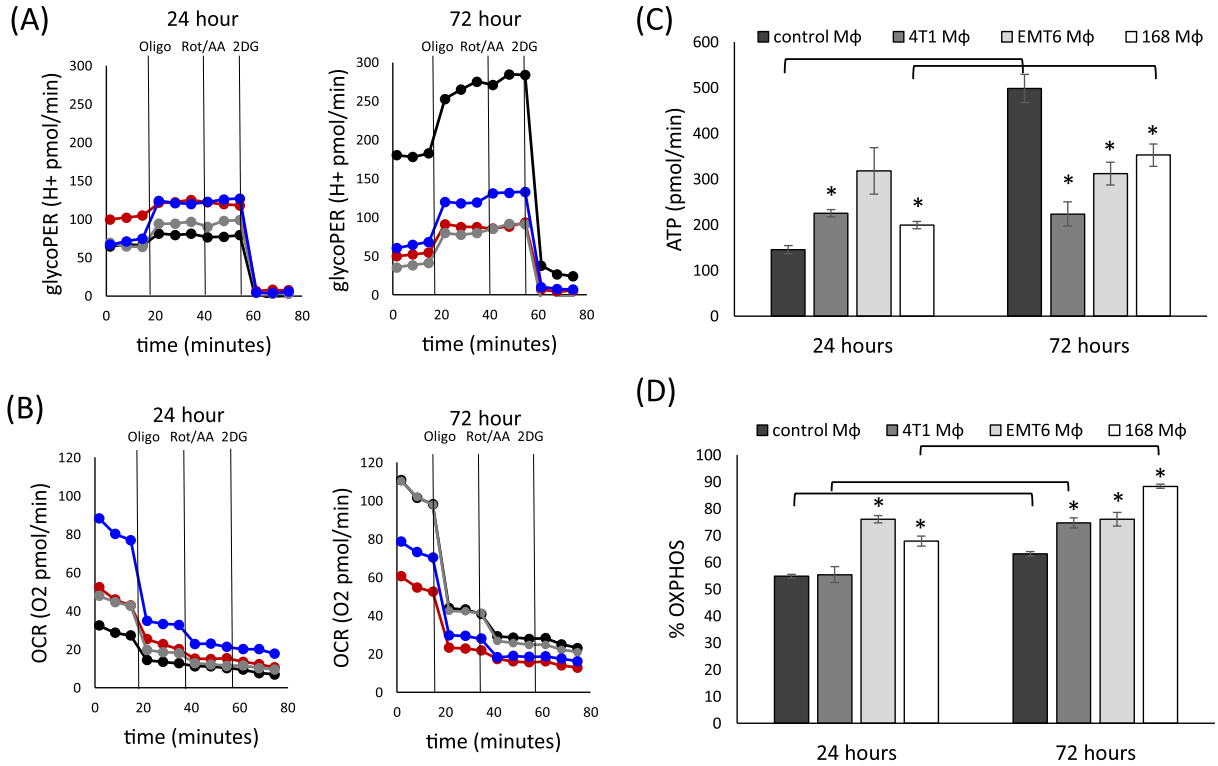

Fig. 6. Analysis of macrophage metabolism at early tumor sites. Seahorse was used to determine the glycolytic proton efflux rate (GlycoPER, A) and oxygen consumption rate (OCR, B) for macrophages collected from **control**, **4T1**, **EMT6** and **168** tumor sites. These data were used to determine the total ATP production rate (C), and % cells using OXPHOS (D). Each experiment was conducted with five mice/set at each time point. All data are the average and standard error of three separate experiments. Where indicated (*) significant differences were found between control and tumor sites $p < 0.05$ using a *Student's t-Test*. Where indicated (⌐) there was a significant change over time $p < 0.05$ using ANOVA.

different parameters including expression of surface markers, cytokines, transcriptional factors, as well as effector function and metabolic profile. We assessed some of these parameters in this study and found a mixed pro- and anti-tumor phenotype, and that some cells showed evidence of moving toward a more pro-tumor phenotype within hours of tumor delivery.

With regard to cytokine expression, macrophages and neutrophils present at the early tumor sites could not be classified as M1/M2 or N1/N2. Within days of tumor delivery macrophages and neutrophils were predominantly producing TNF-α and TGF-β with a minor population of cells producing iNOS and arginase. Surprisingly, the most immunogenic of the tumors (EMT6) showed a significant increase in both pro- and anti-tumor cytokine (arginase, TNF-α, TGF-β) expression within 72 h of tumor delivery. Cytokine expression by myeloid cells at the 4T1 and 168 tumor sites was similar to cytokine expression by myeloid cells at the control site suggesting that cytokine expression at these tumor sites was not influenced by the presence of the tumors. These data indicate that polarization of cytokine expression was not an early event at these murine mammary carcinoma sites. However, while arginase and TGF-β are considered prototypical immune suppressive factors, and iNOS and TNF-α pro-inflammatory factors, the distinction is not always so clear cut. For instance, although TNF-α can help suppress M2 macrophage generation [48], TNF-α can also drive myeloid-derived suppressor cell activity [49], and together with TGF-β induce epithelial-mesenchymal transition [50]. Collectively, these data underscore the difficulty of characterizing myeloid cell phenotype based upon cytokine expression alone.

Phagocytic activity is categorized as an anti-tumor effector function, and inhibition of macrophage-mediated phagocytosis is a characteristic of tumor-induced immune suppression [51,52]. Here we found that only macrophages at the control site exhibited a significant decrease in phagocytic activity. These data may indicate that the presence of the tumors maintained the phagocytic ability of myeloid cells at the early tumor sites, and that inhibition of phagocytic activity is a consequence of later stages of tumor progression.

Similar to phagocytic activity, ROS production has been categorized as an anti-tumor effector function [53], and the majority of myeloid cells at the early tumor sites were ROS^+. However, for neutrophils ROS production may also be considered a pro-tumor marker since release of ROS by neutrophils can suppress T cell proliferation and activation [54], and macrophages become immunosuppressive if treated with ROS [55]. These data illustrate the difficulty of using ROS production to categorize myeloid cells as pro- or anti-tumor. Regardless, here we found that while the majority of macrophages and neutrophils at the early tumor sites were ROS^+, the amount of ROS being produced by these cells was generally lower at 72 h compared to 24 h after tumor delivery. It is interesting to speculate that the decrease in ROS production may be related to alterations in metabolism of the myeloid cells. To address whether there were changes in metabolism we conducted seahorse analysis.

Most data support the contention that M1 macrophages rely more on glycolysis and M2 macrophages rely more on OXPHOS [6–8,41,42]. Using the PyMT mouse breast cancer model Carmona-Fontaine et al. [56] reported that tumor metabolites established gradients of oxygen and lactate that impacted macrophage phenotype. Similarly, Mu et al. [57] reported that lactate from the tumor environment drives the generation of M2 macrophages. Additional factors associated with the tumor environment that can alter macrophage metabolism and function include mTOR [58], HIF1 α [59], PPARγ [60], and glutamine [41]. Data are also accumulating that CD36, which has been used as a marker for M2 macrophages [61], contributes to the generation of pro-tumor macrophages. Huang et al. [62] reported free fatty acid (FFA) uptake via CD36 leads to M2 polarization, and the presence of FFA during macrophage differentiation increased levels of M2 markers such as IL-

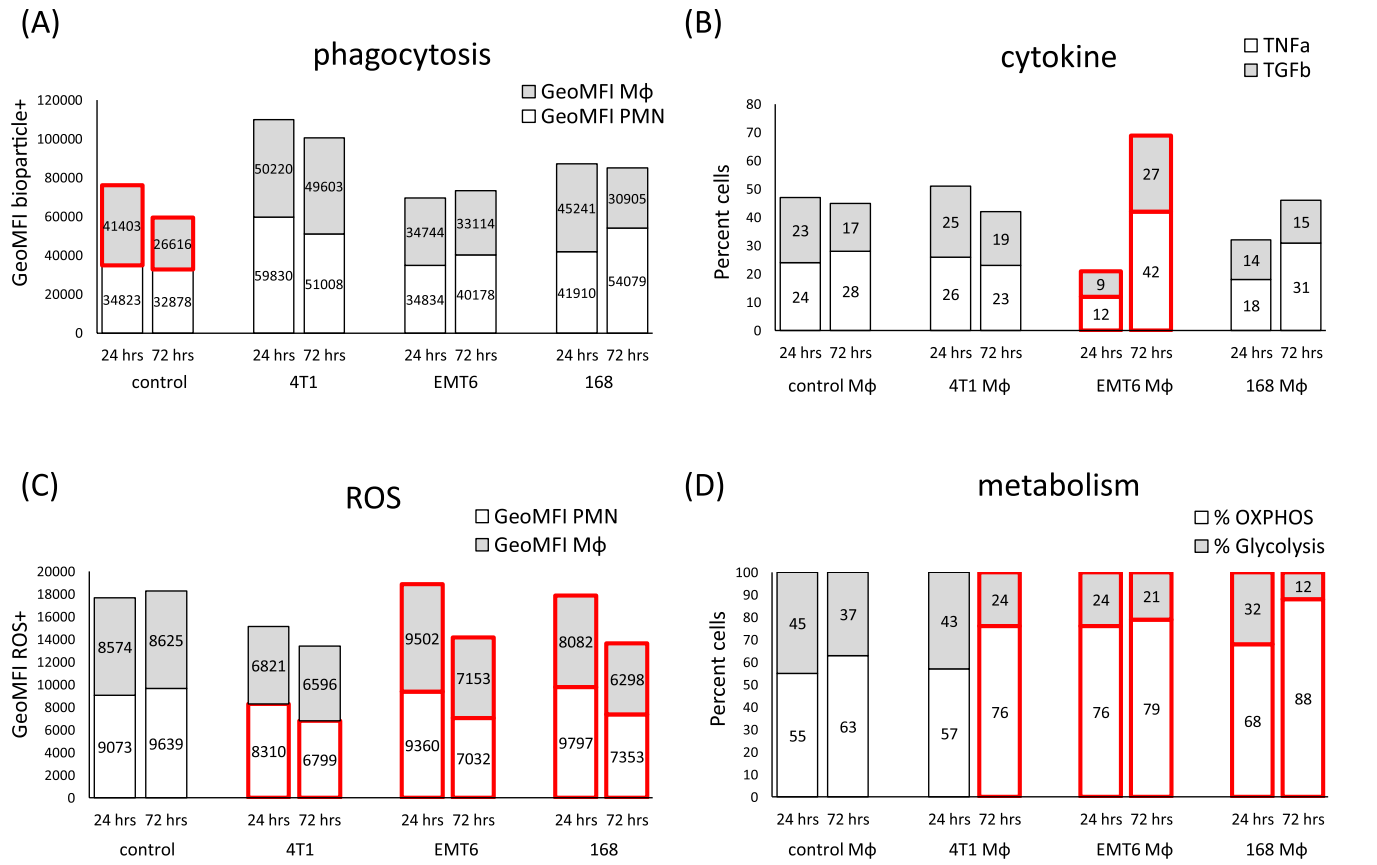

Fig. 7. Summary profile of macrophages and neutrophils present at early tumor sites. There was no significant change over time in the phagocytic capacity of the macrophages or neutrophils at the early tumor sites (A). The only significant change over time in cytokine production was evident in macrophages from the EMT6 tumor site (B). The most significant change over time in ROS production was evident in macrophages from the EMT6 and 168 tumor sites, and neutrophils at all three tumor sites (C). At 24 h macrophages at the EMT6 and 168 tumor sites used significantly more OXPHOS for ATP production than macrophages at the control site, and at 72 h macrophages at all three tumor sites used significantly more OXPHOS for ATP production than macrophages at the control site (D).

10, the mannose receptor, PPAR γ and arginase-1, while there was a decrease in markers associated with M1 macrophages [63]. Significantly, our data show that within 72 h of tumor delivery the macrophages already rely more on OXPHOS than glycolysis. It will be particularly interesting to decipher the mechanism responsible for altered metabolism of the macrophages since we do not anticipate HIF-α, alterations in glutamine, or FFA to be particularly elevated within the first few days after tumor delivery. We are in the process of following expression of a panel of genes that encode proteins associated with glycolysis (IDH, PKM2, HIF1 α) and OXPHOS (AMPK, CARKL, ATP6V, PGC1-b) in an attempt to delineate markers for the early metabolic alterations. It will also be interesting to pursue similar studies in early neutrophils since altered metabolism in neutrophils has been reported in tumor bearing mice and patients with cancer. Using the 4T1 model, Rice et al. [64] reported that low glucose levels contributed to an increase in OXPHOS in tumor associated neutrophils, and they also showed that neutrophils from the blood of patients with ovarian cancer exhibited elevated OXPHOS levels.

In future studies further phenotypic characterization of the early macrophages and neutrophils is warranted. While we focused on F4/80 and Ly6G markers in this study, our preliminary data showed that the majority of early macrophages were Ly6C$^+$, F4/80$^+$ (a more undifferentiated phenotype), and that there was an appreciative level (~20%) of cells that may be categorized as more differentiated macrophages based on morphology and surface staining (F4/80$^+$, Ly6C$^-$). We concentrated on F4/80$^+$ and Ly6G$^+$ cells to capture as many macrophages and neutrophils as possible from the early tumor sites to allow sufficient numbers for functional and metabolic analysis. Yet, since the cytokine, ROS, and phagocytic assays were conducted using flow cytometry we were able to assess whether there were differences if the cells were gated on F4/80^{hi}, F4/80^{lo}, Ly6G^{hi}, and Ly6G^{lo} subpopulations. We found cytokine expression was similar in all subpopulations, while cells expressing high levels of these markers generally expressed more ROS and phagocytic activity than cells expressing low levels of these markers (data not shown). At the very least, future studies need to include additional markers such as CD11b, CD206, and Ly6C for macrophages, and Ly6G in combination with CD11b for neutrophils to delineate when different phenotypic subpopulations of macrophages and neutrophils appear at the early tumor sites.

In addition to elucidating changes in phenotype, function, and metabolism of subsets of macrophages and neutrophils, additional studies need to address whether the macrophages and neutrophils at these early tumor sites impact disease progression. For this purpose adoptive transfer studies or *in vivo* depletion of the cells using antibodies or reagents such as clodronate liposomes would help determine the impact of myeloid cells that arrive at these early tumor sites. Future studies also need to address phenotype, function, and metabolism beyond the 72 h time point, as well as include a more in depth analysis of the macrophages, neutrophils and other white blood cells. For instance, at later time points T cells can be captured and assessed for effector function such as IL-2 production and CTL activity, and co-culture experiments can be used to determine at what point the myeloid cells suppress T cell effector functions. These studies would be particularly interesting because Schietinger et al. [65], using a tamoxifen inducible liver cancer model, reported early (day 8) T cell dysfunction which was not driven by chronic inflammation.

In summary, while a great deal is known about myeloid cells at later stages of disease burden, less is known about these cells at early tumor

sites. This is unfortunate because the early innate immune response to cancer can significantly affect the subsequent adaptive immune response to cancer which is the focus of many immunotherapies. Indeed, the importance of having a thorough understanding of early myeloid cells is underscored by clinical data which reveal macrophages correlate with poor prognosis [1–10], and negatively impact efficacy of checkpoint inhibitor therapy in patients with cancer [11–14]. Our data reveal that distinct innate immune responses to three different murine mammary carcinomas are evident within hours of tumor delivery, and that a mixed phenotype that includes both a pro- and anti-tumor phenotype is evident. Determining when macrophages and neutrophils become fully polarized, and when they begin to contribute to tumor progression may have significant ramifications for monitoring individuals at risk for breast cancer and/or patients diagnosed at early stages of disease.

Acknowledgement

This work was supported by the EXCEL Scholars Program and the Department of Biology at Lafayette College.

References

[1] J.M. Gwak, M.H. Jang, D.I. Kim, A.N. Seo, S.Y. Park, Prognostic value of tumor-associated macrophages according to histologic locations and hormone receptor status in breast cancer, PLoS ONE 10 (2015) 4, https://doi.org/10.1371/journal.pone.0125728.

[2] Z.Y. Yuan, R.Z. Luo, R.J. Peng, S.S. Wang, C. Xue, High infiltration of tumor-associated macrophages in triple negative breast cancer is associated with a higher risk of distant metastasis, Onco. Targets Ther. 7 (2014) 1475–1480.

[3] M. Illemann, O.D. Laerum, J.P. Hasselby, T. Thurison, G. Hoyer-Hansen, H.J. Nielsen, I.J. Christensen, Urokinase-type plasminogen activator receptor (uPAR) on tumor-associated macrophages is a marker of poor prognosis in colorectal cancer, Cancer Med. 3 (2014) 855–864.

[4] K. Gollapudi, C. Galet, T. Grogan, H. Zhang, J.W. Said, J. Huang, D. Elashoff, S.J. Freedland, M. Rettig, W.J. Aronson, Association between tumor-associated macrophage infiltration, high grade prostate cancer, and biochemical recurrence after radical prostatectomy, Am. J. Cancer Res. 3 (2013) 523–529.

[5] X. Zhao, J. Qu, Y. Sun, J. Wang, X. Liu, F. Wang, H. Zhang, W. Wang, X. Ma, X. Gao, S. Zhang, Prognostic significance of tumor-associated macrophages in breast cancer: a meta-analysis of the literature, Oncotarget 8 (2017) 30576–30586.

[6] S.C. Huang, A.M. Smith, B. Everts, M. Colonna, E.L. Pearce, J.D. Schilling, E.J. Pearce, Metabolic reprogramming mediated by the mTORC2-IRF4 signaling axis is essential for macrophage alternative activation, Immunity 45 (2016) 817–830.

[7] E.L. Mills, L.A. O'Neill, Reprogramming mitochondrial metabolism in macrophages as an anti-inflammatory signal, Eur. J. Immunol. 46 (2016) 13–21.

[8] G.M. Tannahill, A.M. Curtis, J. Adamik, E.M. Palsson-McDemott, A.F. McGettrick, G. Goel, C. Frezza, N.J. Bernard, B. Kelly, N.H. Foley, L. Zheng, A. Gardet, Z. Tong, S.S. Jany, S.C. Corr, M. Haneklaus, B.E. Caffrey, K. Pierce, S. Walmsley, F.C. Beasley, E. Cummins, V. Nizet, M. Whyte, C.T. Taylor, H. Lin, S.L. Masters, E. Gottlieb, V.P. Kelly, C. Clish, P.E. Auron, R.J. Xavier, L.A. O'Neill, Succinate is an inflammatory signal that induces IL-1b through HIF1a, Nature 496 (2013) 238–242.

[9] J. Incio, P. Suboj, S.M. Chin, T. Vardam-Kaur, H. Liu, T. Hato, S. Babykutty, I. Chen, V. Deshpande, R.K. Jain, D. Fukumura, Metformin reduces desmoplasia in pancreatic cancer by reprogramming stellate cells and tumor-associated macrophages, e0141392, PLOS One 10 (2015) 12, https://doi.org/10.1371/journal.pone.0141392.

[10] R.J.W. Arts, T.S. Plantinga, S. Tuit, T. Ulas, B. Heinhuis, M. Tesselaar, Y. Sloot, G.J. Adema, L.A.B. Joosten, J.W.A. Smit, M.G. Netea, J.L. Schultze, R.T. Netea-Maier, Transcriptional and metabolic reprogramming induce an inflammatory phenotype in non-medullary thyroid carcinoma-induced macrophages, OncoImmunology 5 (12) (2016) e1229725, https://doi.org/10.1080/2162402X.2016.1229725.

[11] M. Santoni, E. Romagnoli, T. Saladino, L. Foghini, S. Guarino, M. Capponi, M. Giannini, P.D. Cognigni, G. Ferrara, N. Battelli, Triple negative breast cancer: key role of tumor-associated macrophages in regulating the activity of anti-PD-1/PD-L1 agents, Biochim. Biophys. Acta 2018 (1869) 78–84.

[12] S.P. Arlauckas, C.S. Garris, R.H. Kohler, M. Kitaoka, M.F. Cuccarese, K.S. Yang, M.A. Miller, J.C. Carlson, G.J. Freeman, R.M. Anthony, R. Weissleder, M.J. Pittet, In vivo imaging reveals a tumor-associated macrophage-mediated resistance pathway in anti-PD-1 therapy, Sci. Transl. Med. 9 (2017) 389, https://doi.org/10.1126/scitranslmed.aal3604.

[13] L. Cassetta, T. Kitamura, Targeting tumor-associated macrophages as a potential strategy to enhance the response to immune checkpoint inhibitors, Front. Cell Dev. Biol. 6 (2018) 38, https://doi.org/10.3389/fcell.2018.00038.

[14] D. Liu, C. Chang, N. Lu, X. Wang, Q. Lu, X. Ren, P. Ren, D. Zhao, L. Wang, Y. Zhu, F. He, L. Tang, Comprehensive proteomics analysis reveals metabolic reprogramming of tumor-associated macrophages stimulated by the tumor microenvironment, J. Proteom. Res. 16 (2017) 288–297.

[15] T. Chanmee, P. Ontong, K. Konno, N. Itano, Tumor-associated macrophages as major players in the tumor microenvironment, Cancers (Basel) 6 (2014) 1670–1690.

[16] C. Ngambenjawong, H.H. Gustafson, S.H. Pun, Progress in tumor-associated macrophage (TAM)-targeted therapeutics, Adv. Drug Deliv. Rev. 114 (2017) 206–221.

[17] A.R. Poh, M. Ernst, Targeting macrophages in cancer: from bench to bedside, Front. Oncol. 8 (2018) 49, https://doi.org/10.3389/fonc.2018.00049.

[18] B. Kakoschky, T. Pleli, C. Schmithals, S. Zeuzem, B. Brüne, T.J. Vogl, H.W. Korf, A. Weigert, A. Piiper, Selective targeting of tumor associated macrophages in different tumor models, PLoS One 13 (2018) 2, https://doi.org/10.1371/journal.pone.0193015.

[19] C.J. Perry, A.R. Muñoz-Rojas, K.M. Meeth, L.N. Kellman, R.A. Amezquita, D. Thakral, V.Y. Du, J.X. Wang, W. Damsky, A.L. Kuhlmann, J.W. Sher, M. Bosenberg, K. Miller-Jensen, S.M. Kaech, Myeloid-targeted immunotherapies act in synergy to induce inflammation and antitumor immunity, J. Exp. Med. 215 (2018) 877–893.

[20] D. Zhou, C. Huang, Z. Lin, S. Zhan, L. Kong, C. Fang, J. Li, Macrophage polarization and function with emphasis on the evolving roles of coordinated regulation of cellular signaling pathways, Cell Signal. 26 (2014) 192–197.

[21] R. Shrivastava, M. Asif, V. Singh, P. Dubey, S.A. Malik, M.U. Lone, B.N. Tewari, K.S. Baghel, S. Pal, G.K. Nagar, N. Chattopadhyay, S. Bhadauria, M2 polarization of macrophages by Oncostatin M in hypoxic tumor microenvironment is mediated by mTORC2 and promotes tumor growth and metastasis, Cytokine (2018), https://doi.org/10.1016/j.cyto.2018.03.032.

[22] F. Raggi, S. Pelassa, D. Pierobon, F. Penco, M. Gattorno, F. Novelli, A. Eva, L. Varesio, M. Giovarelli, M.C. Bosco, Regulation of human macrophage M1–M2 polarization balance by hypoxia and the triggering receptor expressed on myeloid cells, Front. Immunol. 8 (2017) 1097, https://doi.org/10.3389/fimmu.2017.01097.

[23] N. Dehne, J. Mora, D. Namgaladze, A. Weigert, B. Brüne, Cancer cell and macrophage cross-talk in the tumor microenvironment, Curr. Opin. Pharmacol. 35 (2017) 12–19.

[24] L. Zhu, Q. Zhao, T. Yang, W. Ding, Y. Zhao, Cellular metabolism and macrophage functional polarization, Int. Rev. Immunol. 34 (2015) 82–100.

[25] C. Diskin, E.M. Pålsson-McDermott, Metabolic modulation in macrophage effector function, Front. Immunol. 9 (2018) 270, https://doi.org/10.3389/fimmu.2018.00270.

[26] Y.S. Kim, Y.J. Kim, J.M. Lee, E.K. Kim, Y.J. Park, S.K. Choe, H.J. Ko, C.Y. Kang, Functional changes in myeloid-derived suppressor cells (MDSCs) during tumor growth: FKBP51 contributes to the regulation of the immunosuppressive function of MDSCs, J. Immunol. 188 (2012) 4226–4234.

[27] Z.G. Fridlender, J. Sun, S. Kim, V. Kapoor, G. Cheng, L. Ling, G.S. Worthen, S.M. Albelda, Polarization of tumor-associated neutrophil (TAN) phenotype by TGF-β: "N1" versus "N2" TAN, Cancer Cell 16 (2009) 183–194.

[28] H. Nozawa, C. Chiu, D. Hanahan, Infiltrating neutrophils mediate the initial angiogenic switch in a mouse model of multistage carcinogenesis, PNAS 103 (2006) 124938.

[29] S. Doeber, A.M. Sieuwerts, V. Weerd, H. Stoop, J.W.M. Martens, C.H.M. Deurzen, Gene expression differences between ductal carcinoma in situ with and without progression to invasive breast cancer, Am. J. Path. 187 (2017) 1648–1655.

[30] R. Lesurf, M.R. Aure, H.H. Mork, V. Vitelli, S. Lundgren, A.L. Børresen-Dale, V. Kristensen, F. Wärnberg, M. Hallett, T. Sørlie, Molecular features of subtype-specific progression from ductal carcinoma in situ to invasive breast cancer, Cell Rep. 16 (2016) 1166–1179.

[31] K. Kerlikowske, A.M. Molinaro, M.L. Gauthier, H.K. Berman, F. Waldman, J. Bennington, H. Sanchez, C. Jimenez, K. Stewart, K. Chew, B.M. Ljung, T.D. Tlsty, Biomarker expression and risk of subsequent tumors after initial ductal carcinoma in situ diagnosis, J. Natl. Cancer Inst. 102 (2010) 627–637.

[32] G.T. McKee, G. Tildsley, S. Hammond, Cytologic diagnosis and grading of ductal carcinoma in situ, Cancer 87 (1999) 203–209.

[33] A.C. Degnim, T.L. Hoskin, M. Arshad, M.H. Frost, S.J. Winham, R.A. Brahmbhatt, A. Pena, J.M. Carter, M.L. Stallings-Mann, L.M. Murphy, E.E. Miller, L.A. Denison, C.M. Vachon, K.L. Knutson, D.C. Radisky, D.W. Visscher, Alterations in the immune cell composition in premalignant breast tissue that precede breast cancer development, Clin. Cancer Res. 23 (2017) 3945–3952.

[34] M.J. Campbell, F. Baehner, T. O'Meara, E. Ojukwu, B. Han, R. Mukhtar, V. Tandon, M. Endicott, Z. Zhu, J. Wong, G. Krings, A. Au, J.W. Gray, L. Esserman, Characterizing the immune microenvironment in high-risk ductal carcinoma in situ of the breast, Breast Cancer Res. Treat. 161 (2017) 17–28.

[35] C. Hung, F. Chen, Y. Lin, M. Tsai, S. Wang, Y. Chen, Y. Chen, M. Hou, Altered monocyte differentiation and macrophage polarization patterns in patients with breast cancer, BMC Cancer 18 (2018) 366, https://doi.org/10.1186/s12885-018-4284-y.

[36] V. Riabov, D. Kim, S. Chhina, R.B. Alexander, E.N. Klyushnenkova, Immunostimulatory early phenotype of tumor-associated macrophages does not predict tumor growth outcome in an HLA-DR mouse model of prostate cancer, Cancer Immunol. Immunother. 64 (2015) 873–883.

[37] E.C. Carron, S. Homra, J. Rosenberg, S.B. Coffelt, F. Kittrell, Y. Zhang, C.J. Creighton, S.A. Fuqua, D. Medina, H.L. Machado, Macrophages promote the progression of premalignant mammary lesions to invasive cancer, Oncotarget 8 (2017) 50731–50746.

[38] E.T. Akporiaye, S.J. Stewart, A.P. Stevenson, C.C. Stewart, A gelatin sponge model for studying tumor growth: flow cytometric analysis and quantification of leukocytes and tumor cells in the EMT6 mouse tumor, Cancer Res. 45 (1985) 6457–6462.

[39] R.A. Kurt, J.A. Park, M.C. Panelli, S.F. Schluter, J.J. Marchalonis, B. Carolus, E.T. Akporiaye, T lymphocytes infiltrating sites of tumor rejection and progression

display identical V β usage but different cytotoxic activities, J. Immunol. 154 (1995) 3969–3974.
[40] J.A. Park, R.A. Kurt, R.A. Brown, K.W. Girodino, E.T. Akporiaye, Studies of in vivo recruitment and activation of cytotoxic lymphocytes using a gelatin sponge model of concomitant tumor immunity, Int. J. Cancer 62 (1995) 421–427.
[41] A.K. Jha, S.C. Huang, A. Sergushichev, V. Lampropoulou, Y. Ivanova, E. Loginicheva, K. Chmielewski, K.M. Stewart, J. Ashall, B. Everts, E.J. Pearce, E.M. Driggers, M.N. Artyomov, Network integration of parallel metabolic and transcriptional data reveals metabolic modules that regulate macrophage polarization, Immunity 42 (2015) 419–430.
[42] D. Vats, L. Mukundan, J.I. Odegaard, L. Zhang, K.L. Smith, C.R. Morel, R.A. Wagner, D.R. Greaves, P.J. Murray, A. Chawla, Oxidative metabolism and PGC-1beta attenuate macrophage-mediated inflammation, Cell Metab. 4 (2006) 13–24.
[43] L.A.J. O'Neill, E.J. Pearce, Immunometabolism governs dendritic cell and macrophage function, J. Exp. Med. 213 (2016) 15–23.
[44] C.J. Aslakson, F.R. Miller, Selective events in the metastatic process defined by analysis of the sequential dissemination of subpopulations of a mouse mammary tumor, Cancer Res. 52 (1992) 1399–1405.
[45] S. Ravindranathan, K.G. Nguyen, S.L. Kurtz, H.N. Frazier, S.G. Smith, B.P. Koppolu, N. Rajaram, D.A. Zaharoff, Tumor derived granulocyte colony-stimulating factor diminished efficacy of breast tumor cell vaccines, Breast Cancer Res. 20 (2018), https://doi.org/10.1186/s13058-018-1054-3.
[46] A. Shapouri-Moghaddam, S. Mohammadian, H. Vazini, M. Taghadosi, S.A. Esmaeili, F. Mardani, B. Seifi, A. Mohammadi, J.T. Afshari, A. Sahebkar, Macrophage plasticity, polarization, and function in health and disease, J. Cell. Phys. 233 (2018) 6425–6440.
[47] I. Mishalian, R. Bayuh, L. Levy, L. Zolotarov, J. Michaeli, Z.G. Fridlender, Tumor-associated neutrophils (TAN) develop pro-tumorigenic properties during tumor progression, Cancer Immunol. Immunother. 62 (2013) 1745–1756.
[48] F. Kratochvill, G. Neale, J.M. Haverkamp, L.A. Van de Velde, A.M. Smith, D. Kawauchi, J. McEvoy, M.F. Roussel, M.A. Dyer, J.E. Qualls, P.J. Murray, TNF counterbalances the emergence of M2 tumor macrophages, Cell Rep. 12 (2015) 1902–1914.
[49] M. Schroder, M. Krotschell, L. Conrad, S.K. Naumann, C. Bachran, A. Rolfe, V. Umansky, L. Helming, L.K. Swee, Genetic screening in myeloid cells identifies TNF-a autocrine secretion as a factor increasing MDSC suppressive activity via Nos-2 up-regulation, Sci. Rep. 8 (2018) 13399, https://doi.org/10.1038/s41598-018-31674-1.
[50] M.K. Asiedu, J.N. Ingle, M.D. Behrens, D.C. Radisky, K.L. Knutson, TGFbeta/TNF (alpha)-mediated epithelial-mesenchymal transition generates breast cancer stem cells with a claudin-low phenotype, Cancer Res. 71 (2011) 4707–4719.
[51] P. Cabrales, RRx-001 acts as a dual small molecule checkpoint inhibitor by down-regulating CD47 on cancer cells and SIRPa on monocytes/macrophages, Trans. Oncol. 12 (2019) 626–632.
[52] M.N. McCracken, A.C. Cha, I.L. Weissman, Molecular pathways: activating T cells after cancer cell phagocytosis from blockade of CD47 “Don't Eat Me” signals, Clin. Cancer Res. 21 (2015) 3597–3601.
[53] F. Huang, J. Zhao, L. Wang, C. Gao, S. Liang, D. An, J. Bai, Y. Chen, H. Han, H. Qin, miR-148a-3p mediates notch signaling to promote the differentiation and M1 activation of macrophages, Front. Immunol. 8 (2017) 1327, https://doi.org/10.3389/fimmu.2017.01327.
[54] J. Pillay, V.M. Kamp, E. van Hoffen, T. Visser, T. Tak, J.W. Lammers, L.H. Ulfman, L.P. Leenen, P. Pickkers, L. Koenderman, A subset of neutrophils in human systemic inflammation inhibits T cell responses through Mac-1, J. Clin. Invest. 122 (2012) 327–336.
[55] C. Roux, S.M. Jafari, R. Shinde, G. Duncan, D.W. Cescon, J. Silvester, M.F. Chu, K. Hodgson, T. Berger, A. Wakeham, L. Palomero, M. Garcia-Valero, M.A. Pujana, T.W. Mak, T.L. McGaha, P. Cappello, C. Gorrini, Reactive oxygen species modulate macrophage immunosuppressive phenotype through the up-regulation of PD-L1, PNAS (2019), https://doi.org/10.1073/pnas.1819473116.
[56] C. Carmona-Fontaine, M. Deforet, L. Akkari, C.B. Thompson, J.A. Joyce, J.B. Xavier, Metabolic origins of spatial organization in the tumor microenvironment, PNAS 114 (2017) 2934–2939.
[57] X. Mu, W. Shi, Y. Xu, C. Xu, T. Zhao, B. Geng, J. Yang, J. Pan, S. Hu, C. Zhang, J. Zhang, C. Wang, J. Shen, Y. Che, Z. Liu, Y. Lv, H. Wen, Q. You, Tumor-derived lactate induces M2 macrophage polarization via the activation of the ERK/STAT3 signaling pathway in breast cancer, Cell Cycle 17 (2018) 428–438.
[58] M. Wenes, M. Shang, M. Di Matteo, J. Goveia, R. Martin-Perez, J. Serneels, H. Prenen, B. Ghesquière, P. Carmeliet, M. Mazzone, Macrophage metabolism controls tumor blood vessel morphogenesis and metastasis, Cell Metab. 24 (2016) 701–715.
[59] R.J. Arts, T.S. Plantinga, S. Tuit, T. Ulas, B. Heinhuis, M. Tesselaar, Y. Sloot, G.J. Adema, L.A. Joosten, J.W. Smit, M.G. Netea, J.L. Schultze, R.T. Netea-Maier, Transcriptional and metabolic reprogramming induce an inflammatory phenotype in non-medullary thyroid carcinoma-induced macrophages, OncoImmunology 5 (2016), https://doi.org/10.1080/2162402X.2016.1229725.
[60] X. Deng, P. Zhang, T. Liang, S. Deng, X. Chen, L. Zhu, Ovarian cancer stem cells induce the M2 polarization of macrophages through the PPARγ and NF-κB pathways, Int. J. Mol. Med. 36 (2015) 449–454.
[61] A. Mantovani, S. Sozzani, M. Locati, P. Allavena, A. Sica, Macrophage polarization: tumor-associated macrophages as a paradigm for polarized M2 mononuclear phagocytes, Trends Immunol. 23 (2002) 549–555.
[62] S.C. Huang, B. Everts, T. Ivanova, D. O'Sullivan, M. Nascimento, A.M. Smith, W. Beatty, L. Love-Gregory, W.Y. Lam, C.M. O'Neill, C. Yan, H. Du, N.A. Abumrad, J.F. Urban, M.N. Artyomov, E.L. Pearce, E.J. Pearce, Cell-intrinsic lysosomal lipolysis is essential for alternative activation of macrophages, Nat. Immunol. 15 (2014) 846–855.
[63] F.J. Rios, M.M. Koga, M. Pecenin, M. Ferracini, M. Gidlund, S. Jancar, Oxidized LDL induces alternative macrophage phenotype through activation of CD36 and PAFR, Mediators Inflamm. 2013 (2013) 198193, , https://doi.org/10.1155/2013/198193.
[64] C.M. Rice, L.C. Davies, J.J. Subleski, N. Maio, M. Gonzalez-Cotto, C. Andrews, N.L. Patel, E.M. Palmieri, J.M. Weiss, J. Lee, C.M. Annunziata, T.A. Rouault, S.K. Durum, D.W. McVicar, Tumour-elicited neutrophils engage mitochondrial metabolism to circumvent nutrient limitations and maintain immune suppression, Nat. Comm. 9 (2018) 5099, https://doi.org/10.1038/s41467-018-07505-2.
[65] A. Schietinger, M. Philip, V.E. Krisnawan, E.Y. Chiu, J.J. Delrow, R.S. Basom, P. Lauer, D.G. Brockstedt, S.E. Knoblaugh, G.J. Hämmerling, T.D. Schell, N. Garbi, P.D. Greenberg, Tumor-specific T cell dysfunction is a dynamic antigen-driven differentiation program initiated early during tumorigenesis, Immunity 45 (2016) 389–401.